

# Dosimetric modeling of the microselectron high-dose rate $^{192}\text{Ir}$ source by the multigroup discrete ordinates method

George M. Daskalov<sup>a)</sup>

National Research Council of Canada, IRS/INMS, 1500 Montreal Rd., Ottawa, ON K1A 0R6, Canada

R. S. Baker

Los Alamos National Laboratory, MS D409, Los Alamos, New Mexico 87545

D. W. O. Rogers

National Research Council of Canada, IRS/INMS, 1500 Montreal Rd., Ottawa, ON K1A 0R6, Canada

J. F. Williamson

Washington University Medical School, Radiation Oncology Physics 510 S. Kingshighway Boul., St. Louis, Missouri 63110

(Received 10 November 1999; accepted for publication 31 May 2000)

The DANTSYS multigroup discrete ordinates computer code is applied to quantitatively estimate the absorbed dose rate distributions in the vicinity of a microSelectron  $^{192}\text{Ir}$  high-dose-rate (HDR) source in two-dimensional cylindrical  $R$ - $Z$  geometry. The source is modeled in a cylindrical water phantom of diameter 20 cm and height 20 cm. The results are also used for evaluation of the Task Group 43 (TG-43) dosimetric quantities. The DANTSYS accuracy is estimated by direct comparisons with corresponding Monte Carlo results. Our 210-group photon cross section library developed previously, together with angular quadratures consisting of 36 ( $S_{16}$ ) to 210 ( $S_{40}$ ) directions and associated weights per octant, are used in the DANTSYS simulations. Strong ray effects are observed but are significantly mitigated through the use of DANTSYS's stochastic ray-tracing first collision source algorithm. The DANTSYS simulations closely approximate Monte Carlo estimates of both direct dose calculations and TG-43 dosimetric quantities. The discrepancies with  $S_{20}$  angular quadrature (55 directions and weights per octant) or higher are shown to be less than  $\pm 5\%$  (about 2.5 standard deviations of Monte Carlo calculations) everywhere except for limited regions along the  $Z$  axis of rotational symmetry, where technical limitations in the DANTSYS first collision source implementation makes adequate suppression of ray effects difficult to achieve. The efficiency of DANTSYS simulations is compared with that of the EGS4 Monte Carlo code. It is demonstrated that even with the 210-group cross section library, DANTSYS achieves two-fold efficiency gains using the  $S_{20}$  quadrature set. The potential of discrete ordinates method for further efficiency improvements is also discussed. [S0094-2405(00)01510-8]

Key words: multigroup discrete ordinates photon transport, Monte Carlo photon transport, photon kerma, absorbed dose, microSelectron Ir-192 HDR source, brachytherapy dosimetry

## I. INTRODUCTION

The Discrete Ordinates Method (DOM)<sup>1</sup> is a deterministic solution of the Boltzmann transport equation governing particle transport. The method is well known and routinely used for reactor physics applications.<sup>1,2</sup> However, DOM is rarely applied to medical radiation physics problems, where Monte Carlo solutions of the Boltzmann equation are almost universally used. Since DOM (as used here) is fundamentally formulated as a finite-difference equation (rather than as finite differencing of an analytic approximation), few approximations are made. Thus DOM solutions will approach the exact solution of the Boltzmann equation as the space, energy, and angle meshes approach differential size. Similar to Monte Carlo applications in brachytherapy, DOM can account for tissue composition, applicator attenuation, and intersource attenuation. It provides an alternative to Monte Carlo solutions of the transport equation. The major differences between discrete ordinates calculations and Monte Carlo simulations are as follows.

- (i) DOM is a nonstochastic technique, and flux errors are systematic rather than statistical.
- (ii) DOM automatically provides the complete two- or three-dimensional flux and kerma distributions.
- (iii) DOM uses a mesh-based rather than analytic description of the problem geometry.

In addition, DOM solutions can benefit from information derived from similar problems solved previously. DOM's mesh-based geometry representation is well suited for use with CT- and MRI- defined patient geometries. Material properties can vary from one voxel to another. Usually, fluxes are calculated at the center of each mesh cell used to describe the problem geometry. Although, in principle, DOM can be used to solve the coupled photon-electron transport problems,<sup>3</sup> the code we have investigated is designed for modeling transport of indirectly ionizing radiation, and is therefore a potentially useful dose computation tool in low-energy x-ray therapy and brachytherapy, where

secondary charged particle equilibrium is a valid approximation.<sup>4</sup> The goal of this study is to demonstrate the accuracy with which DOM can evaluate dose distributions in brachytherapy.

In radiotherapy, DOM has been applied to boron neutron-capture therapy (BNCT),<sup>5–8</sup> Cf-252 source dosimetry,<sup>9,10</sup> fast neutron beam characterization,<sup>11</sup> and medical accelerators neutron leakage evaluation.<sup>12</sup> Until recently,<sup>13,14</sup> however, DOM has not been applied to brachytherapy problems in multidimensional geometries. The characteristics of this application, i.e., small discrete sources emitting low-energy photons that are embedded in shallow penetration media differ significantly from high-energy photon, deep penetration problems where DOM has been validated. Previously, we demonstrated that DOM kerma-rate distributions accurately reproduced Monte Carlo photon transport (MCPT) simulations for a broad range of photon spectra and idealized brachytherapy geometries provided that an appropriate multigroup cross section library is used together with a suitable choice of the other computational parameters.<sup>13,14</sup>

Our previous work in applying DOM to brachytherapy dosimetry considered only highly simplified spherical and cylindrical sources. In contrast, the present study is the first to use the standard DOM photon transport code DANTSYS<sup>15</sup> to evaluate the complete two-dimensional (2D) dose-rate distribution around an actual clinical source, the microSelectron high-dose-rate (HDR) Ir-192 source. The dose-rate constant

and the other dosimetric quantities recommended by the AAPM Task Group 43<sup>16</sup> (TG-43) are also evaluated, requiring a DOM estimate of the source's air-kerma strength per unit activity ratio. Finally, this work provides the first complete mathematical description of the multigroup discrete ordinates transport solution in the medical physics literature. A major goal of this study is to demonstrate the accuracy of discrete ordinates calculations, in a clinically realistic geometry, by means of a direct comparison with Monte Carlo simulations. The effects of important computational parameters, such as replacing discrete primary photon sources with a precalculated first collision source, for cost effective ray effects mitigation, and the angular quadratures used are also discussed. Finally, an assessment of the DANTSYS efficiency relative to Monte Carlo is made.

## II. MATERIALS AND METHODS

### A. Discrete ordinates method for solving the transport equations

The distribution of neutral particle radiation in a system of photon sources and absorbing media can be described by the Boltzmann transport equation.<sup>1</sup> For brevity we limit ourselves to one-dimensional slab geometry, in which case the time-independent transport equation becomes

$$\underbrace{\eta \frac{\partial}{\partial x} \psi(x, E, \eta)}_{T_1} + \underbrace{\mu_t(x, E) \psi(x, E, \eta)}_{T_2} = \underbrace{\int_{-1}^1 d\eta' \int_0^{E_0} dE' \mu_s(x, E' \rightarrow E; \eta_0) \psi(x, E', \eta')}_{T_3} + \underbrace{S(x, E, \eta)}_{T_4} \quad (1)$$

where  $\psi(x, E, \eta)$  is the angular particle flux (e.g., photons per cm<sup>2</sup> per s) at location  $x$  with energy  $E$  per unit solid angle and energy, and  $\eta$  denotes the direction cosine of the particle trajectory with respect to the  $X$  axis. This complex equation in three independent variables (six in the general three-dimensional case) states that the change in flux  $\eta(\partial/\partial x)\psi(x, E, \eta)$  (denoted by  $T_1$ ) in any phase space cell,  $dx dE d\eta$ , is a sum of (i) losses to photon attenuation ( $T_2$ ); (ii) gains due to in-scattering from other energies and angles ( $T_3$ ); and (iii) contributions from any photon sources,  $S(x, E, \eta)$  in units of particles per unit volume, solid angle, and energy, per s ( $T_4$ ). The quantities  $\mu_t(x, E)$  and  $\mu_s(x, E' \rightarrow E; \eta_0)$  are the macroscopic total and scattering cross sections, respectively, and  $\eta_0$  denotes the cosine of the scattering angle (between the incident and scattered particle direction). From the angular flux, all radiological quantities of interest, e.g. dose rates, can be calculated (neglecting secondary electrons),

$$\begin{aligned} \dot{D}(x) \cong \dot{K}(x) &= 2\pi \int_{-1}^1 d\eta \int_0^{E_0} dE (\mu_{en}/\rho)(x, E) E \psi(x, E, \eta) \\ &\equiv \int_0^{E_0} dE (\mu_{en}/\rho)(x, E) E \Phi(x, E), \end{aligned} \quad (2)$$

where  $\Phi(x, E) \equiv 2\pi \int_{-1}^1 d\eta \psi(x, E, \eta)$  is the one-dimensional scalar flux, and  $E_0$  denotes the maximum energy of the photons emitted by the sources.

The core of the discrete ordinates method is the discretization of the angular variable  $\eta$  in Eq. (1). An important intermediate step is to approximate the angular dependency of the differential cross sections  $\mu_s$  by a truncated Legendre polynomial series. The Legendre polynomials form a complete set of orthogonal functions on the segment  $[-1, 1]$ .<sup>1</sup> The orthogonality relations are given by

$$\int_{-1}^1 dx P_n(x)P_m(x) = \begin{cases} 2, & n = m; \\ 0, & n \neq m, \end{cases} \quad (3)$$

where  $P_n(x)$ ,  $P_m(x)$  denote Legendre polynomials of degree  $n$  and  $m$ , respectively.

The expansion of  $\mu_s$  takes the form<sup>1</sup>

$$\mu_s(x, E' \rightarrow E, \eta_0) \cong \frac{1}{2} \sum_{n=0}^N \mu_s^n(x, E' \rightarrow E) P_n(\eta_0). \quad (4)$$

The completeness of the expansion, Eq. (4), is expressed by the fact that it is *exact*, provided that  $N \rightarrow \infty$ , however, one usually restricts the expansion to finite values of  $N$ , traditionally denoted as  $P_N$ .

From Eq. (4), and Eq. (3), the expansion coefficients (or moments) are obtained by

$$\mu_s^n(x, E' \rightarrow E) \cong (2n + 1) \int_{-1}^1 d\eta_0 \mu_s(x, E' \rightarrow E, \eta_0) P_n(\eta_0). \quad (5)$$

In this study we demonstrate that  $N=3$  is a sufficiently accurate approximation.<sup>13,14</sup>

Substituting Eq. (4) into Eq. (1), and using the addition theorem for the Legendre polynomials,<sup>1</sup>

$$P_n(\eta_0) = P_n(\eta)P_n(\eta'), \quad (6)$$

where  $\eta'$  and  $\eta$  denote the incident and scattered direction cosines, respectively, we obtain

$$\underbrace{\eta \frac{\partial}{\partial x} \psi(x, E, \eta)}_{T_1} + \underbrace{\mu_t(x, E) \psi(x, E, \eta)}_{T_2} = \underbrace{\sum_{n=0}^N \frac{1}{2} \int_0^{E_0} dE' \mu_s^n(x, E' \rightarrow E) P_n(\eta) \psi^n(x, E')}_{T_3} + \underbrace{S(x, E, \eta)}_{T_4} \quad (7)$$

where

$$\psi^n(x, E') = \int_{-1}^1 d\eta' \psi(x, E', \eta') P_n(\eta') \quad (8)$$

are the angular flux moments.

The discrete ordinates approximation consists of requiring Eq. (7) to hold only for  $M$  discrete directions  $\eta_m$ , leading to

$$\underbrace{\eta_m \frac{\partial}{\partial x} \psi_m(x, E)}_{T_1} + \underbrace{\mu_t(x, E) \psi_m(x, E)}_{T_2} = \underbrace{\sum_{n=0}^N \frac{1}{2} \int_0^{E_0} dE' \mu_s^n(x, E' \rightarrow E) P_n(\eta_m) \psi^n(x, E')}_{T_3} + \underbrace{S(x, E, \eta_m)}_{T_4} \quad (9)$$

where  $\psi_m(x, E) = \psi(x, E, \eta_m)$ , and it is assumed that the interval  $-1 \leq \eta \leq 1$  is partitioned into  $M$  ordinates  $\eta_m$ . Simultaneously, the angular flux moments  $\psi^n$ , defined in Eq. (8), are approximated by a finite sum or quadrature formula,

$$\psi^n(x, E') \cong \sum_{m=1}^M w_m \psi_m(x, E') P_n(\eta_m), \quad n = 0, 1, 2, \dots, N, \quad (10)$$

where the weights  $w_m$  are associated with each discrete direction  $\eta_m$ . The combination of the discrete direction cosines together with their associated weights is referred to as a ‘‘quadrature set.’’ In the literature the order of expansion,  $M$ , is represented by the notation  $S_N$ . The relationship between the subscript  $N$  (not related to  $N$  in the  $P_N$  notation above) and the actual number of angles and weights depends on the symmetries assumed by the quadrature derivation.

Substituting Eq. (10) in Eq. (9), we obtain the discrete ordinates equations,

$$\underbrace{\eta_m \frac{\partial}{\partial x} \psi_m(x, E)}_{T_1} + \underbrace{\mu_t(x, E) \psi_m(x, E)}_{T_2} = \underbrace{\sum_{n=0}^N \frac{1}{2} \int_0^{E_0} dE' \mu_s^n(x, E' \rightarrow E) P_n(\eta_m) \sum_{m'=1}^M w_{m'} \psi_{m'}(x, E') P_n(\eta_{m'})}_{T_3} + \underbrace{S(x, E, \eta_m)}_{T_4}, \quad m = 1, 2, \dots, M. \quad (11)$$

Equation (11) forms the foundation of the discrete ordinates method's implementation for solving the transport equations. The choice of the discrete directions  $\eta_m$  and corresponding weights  $w_m$  seeks to satisfy the following conditions: (i) physical symmetries are preserved upon discretization; (ii) the angular moments [e.g., Eqs. (8),(10)] accurately represents the problem sources; and (iii) the derivatives with respect to angle (in curved geometries) are approximated in a simple manner.

In multidimensional geometries, not all of the above conditions can be met exactly with a single selection of a discrete ordinate set, and compromises are made. A complete discussion regarding various quadrature sets and their implementation can be found in the work of Alcouffe and O'Dell.<sup>2</sup>

To solve Eq. (11) the remaining independent variables,  $x$  and  $E$ , must be discretized. Modern discrete ordinates codes (including the DANTSYS code used in this study) invoke the multigroup energy approximation. In this approach, the energy domain  $(0, E_0)$  is partitioned into  $G$  intervals of width  $\Delta E = E_g - E_{g+1}$ ,  $g = 1, \dots, G$  containing those particles with energies between  $E_g$  and  $E_{g+1}$ . By convention,  $E_1 = E_0$ ,  $E_{G+1} = 0$ , implying that when the group index  $g$  increases, the energy associated with the group  $g$  decreases. The group angular flux is defined as

$$\psi_{m,g}(x) \equiv \int_{E_{g+1}}^{E_g} dE \psi(x, E, \eta_m) = \int_{\Delta E_g} dE \psi_m(x, E). \quad (12)$$

The group flux  $\psi_{m,g}(x)$  is no longer a distribution in energy or an average in energy but is the total number of particles in the energy interval  $\Delta E_g$  traveling in a direction defined by  $\eta_m$ . Therefore, integrals over energy, e.g.,  $\int_0^{E_0} F(E') dE'$ , can be replaced with sums of the form  $\sum_{g'=1}^G \int_{\Delta E_{g'}} F(E') dE'$ . The multigroup energy approximation is introduced in Eq. (11) by multiplying the equation by  $dE$  and integrating over each group bin  $\Delta E_g$ .

To complete the integration of Eq. (11), for simplicity suppose that within each group  $\Delta E_g (g = 1, \dots, G)$  the angular flux can be approximated by

$$\psi_m(x, E) \approx \psi_{m,g}(x) f(E), \quad (13)$$

where  $f(E)$  is some known function of energy. In the multigroup theory,  $f(E)$  is called the weighting function. From the definition of the group flux, Eq. (12), it follows that in each energy interval  $f(E)$  is normalized according to

$$\int_{\Delta E_g} f(E) dE = 1, \quad g = 1, \dots, G. \quad (14)$$

Carrying out the integration of Eq. (11) over  $\Delta E_g$  and using the separability assumption, Eq. (13), we obtain

$$\underbrace{\eta_m \frac{\partial}{\partial x} \psi_{m,g}(x)}_{T_1} + \underbrace{\mu_{t,g}(x) \psi_{m,g}(x)}_{T_2} = \underbrace{\frac{1}{2} \sum_{n=0}^N \sum_{g'=1}^G \mu_{s,g' \rightarrow g}^n(x) P_n(\eta_m) \sum_{m'=1}^M w_{m'} \psi_{m',g'}(x) P_n(\eta_{m'})}_{T_3} + \underbrace{S_{m,g}(x)}_{T_4}, \quad m = 1, 2, \dots, M; \quad g = 1, \dots, G, \quad (15)$$

where  $S_{m,g}(x, \eta_m) = \int_{\Delta E_g} dE S(x, E, \eta_m)$  is the number of particles emitted in group  $g$  in direction  $\eta_m$  per unit volume by the external sources at position  $x$ , and

$$\mu_{t,g}(x) = \int_{\Delta E_g} dE \mu_t(x, E) f(E),$$

$$\mu_{s,g' \rightarrow g}^n(x) = \int_{\Delta E_g} dE \int_{\Delta E_{g'}} dE' \mu_s^n(x, E' \rightarrow E) f(E'), \quad (16)$$

are the multigroup cross sections.

Equation (15) represents  $G \times M$  multigroup discrete ordinates coupled equations in one-dimensional Cartesian geometry. The coupling occurs due to the presence of the scattering term  $T_3$ , which defines the dependency of the group  $g$  flux on the fluxes in other groups  $g'$ . Identification of the spectral weighting function,  $f(E)$ , is not straightforward

since the flux spectrum has a complex dependence on the geometry and physical properties of the system under consideration. However, when the number of energy groups is sufficiently large and the energy group widths are sufficiently narrow, the group cross sections approximate the continuous energy cross sections and have little dependence on the weighting functions used.<sup>1,17</sup> Under such circumstances the use of analytic or semianalytic weighting functions is justified and leads to spectrum-independent multigroup cross section libraries.

Equations (15) are solved successively for each energy group, one at a time, starting with group  $g = 1$ , which contains photons only in the highest-energy band and has no in-scattering ( $T_3 = 0$  for all  $g'$  except for  $g' = g = 1$ , the in-group scattering or scattering without change of energy group). The group flux  $\psi_{m,1}$  is then calculated. The scattering contribution of  $\psi_{m,1}$  to  $\psi_{m,2}$ ,  $\psi_{m,3}$ , and so on, is calculated

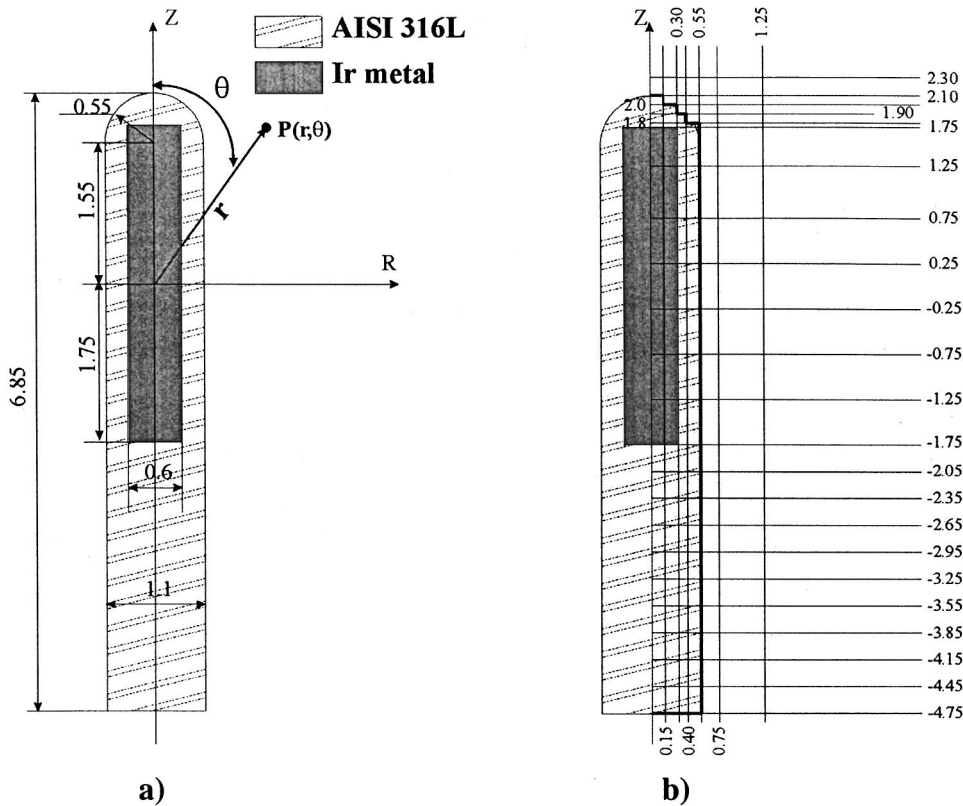


FIG. 1. The geometry used for modeling of the <sup>192</sup>Ir HDR source by MCPT (a) and DANTSYS (b). Material composition: core—pure iridium metal (density,  $\rho=22.42 \text{ g cm}^{-3}$ ) with uniformly distributed radioactive <sup>192</sup>Ir throughout its volume; AISI316L steel capsule by weight —2% Mn, 1% Si, 17% Cr, 12% Ni, and 68% Fe, with a density of  $\rho=8.02 \text{ g cm}^{-3}$ . All sizes are in mm.

and treated like a contribution to the respective group source terms  $S_{m,2}$ ,  $S_{m,3}$ , etc. This process continues for groups 2,3,...,G. To solve Eqs. (15) within each group, the spatial  $x$  domain is discretized into  $I$  intervals (called mesh cells in multidimensional problems)  $\Delta x_i = x_{i+1/2} - x_{i-1/2}$ ,  $i = 1, \dots, I$ , with  $x_{1/2}$  coinciding with the boundary  $x=0$  (“left” boundary), and  $x_{I+1/2}=a$ , where  $a$  is the maximal size of the system (“right” boundary). Different properties, i.e.,  $\mu_t$  and  $\mu_s$ , can be assigned to each interval, thus allowing arbitrary complex inhomogeneous geometries to be modeled. The spatial derivatives are replaced by finite differences:

$$\frac{\partial \psi_{m,g}(x_i)}{\partial x} \approx \frac{\psi_{m,g}(x_{i+1/2}) - \psi_{m,g}(x_{i-1/2})}{\Delta x_i},$$

$$x_i = \frac{1}{2}(x_{i+1/2} + x_{i-1/2}). \tag{17}$$

The “centered,”  $\psi_{m,g}(x_i)$ , and “end point,”  $\psi_{m,g}(x_{i\pm 1/2})$ , fluxes introduced in Eq. (17) are further related in a consistent fashion by supplementary equations<sup>1,2,18</sup> to obtain a closed set of  $2IM$  simultaneous equations within each group  $g$  that are solved iteratively. The iterations are necessary since the contribution of in-group scattering for each group  $g'=g$  (term  $T_3$ ) is as yet unknown. Therefore, the solution begins with an estimate of  $\psi_{m,g}(x)$ , say  $\psi_{m,g}^0(x)$ , which is progressively refined with each subsequent iteration  $k$ . This process continues until the iteration convergence criterion is satisfied, e.g.,

$$\max_x |\Phi_g^{k+1}(x) - \Phi_g^k(x)| \leq \epsilon, \tag{18}$$

where  $\Phi_g^k(x)$  is the scalar flux [as defined after Eq. (2)] for group  $g$  at  $x$  after the  $k$ -th iteration, and  $\epsilon$  is typically taken between 0.001 and 0.0001. The process starts at one corner of the  $x-\eta$  mesh, e.g.  $(x_1, \eta_1)$ , whereby applying the boundary conditions, the difference equation (17) can be solved for the next value,  $(x_2, \eta_1)$ . The process continues across the mesh in a systematic way, recursively calculating one  $\psi_{m,g}(x)$  after another. The convergence, freedom from negative flux artifacts and accuracy<sup>1,2,18</sup> achieved by DOM are very sensitive to the details of mesh differencing and sweeping. The CPU time required is roughly proportional to the number of phase space cells (space, angle, and energy) times the number of iterations in each energy group and the order of Legendre polynomial expansion.

Once the calculations are completed, and the group fluxes are known, the dose rate, Eq. (2), can be evaluated by

$$\dot{D}(x_i) = \sum_{g=1}^G \sum_{m=1}^M w_m \bar{E}_g \psi_{m,g}(x_i) (\mu_{en}/\rho)_g(x_i), \tag{19}$$

at each point  $x_i$  of the spatial lattice.  $(\mu_{en}/\rho)_g(x_i)$  ( $g = 1, \dots, G$ ) denotes appropriate group mass-energy absorption factors (called group kerma factors), and  $\bar{E}_g = \frac{1}{2}(E_g + E_{g+1})$  is the average energy of group  $g$ . The derivation of multidimensional discrete ordinates equations is conceptually similar but more complex.<sup>1,2</sup>

In multidimensional geometries, the concentrated streaming of particles along discrete angular directions leads to nonphysical fluctuations of the flux known as ray effects.<sup>1,2</sup> Ray effects tend to have the largest impact in two- and three-dimensional problems with localized sources, where the ef-

fect of scattered radiation is comparable to that of the primary particles (those originating from the sources), which is essentially the case in brachytherapy. Increasing the number of discrete directions better approximates the true physical situation of continuous angular variables and naturally mitigates the ray effects. This approach, however, leads to highly intensive and costly calculations.<sup>1,2</sup> It is demonstrated later in this study that implementing a first collision source mitigation technique sufficiently reduces the impact of ray effects on the accuracy of the DOM for brachytherapy calculations and allows the use of lower-order angular quadratures with the same finite-difference geometry representation.

## B. Computational details

### 1. Monte Carlo calculations and AAPM Task Group 43 formalism

We used a continuous energy Monte Carlo photon transport (MCPT) code<sup>19–23</sup> to calculate the dose rate distributions around the microSelectron <sup>192</sup>Ir high dose-rate (HDR) source. These results constitute a “gold standard” for evaluating the accuracy of the corresponding discrete ordinates simulations. Figure 1(a) shows the underlying geometry and material composition of the source used in our MCPT calculations.<sup>23</sup> The primary photon spectrum for <sup>192</sup>Ir was that of Glasgow and Dilman.<sup>24</sup> The source is placed at the center of a cylindrical water phantom of diameter 20 cm and height 20 cm. The photon cross section library DLC-146<sup>25</sup> was used and included coherent and incoherent scattering as well photoelectric absorption. Since characteristic x-ray production was not included in the DOM multigroup library, it was removed from our MCPT simulations as well. The mass energy absorption coefficients of Hubbell and Seltzer<sup>26</sup> were used to convert the photon energy flux into collision kerma, consistent with the DLC-146 data. Since our MCPT code does not model transport and scattering of secondary electrons, collision kerma is used to approximate an absorbed dose since for the low-energy photons emitted by <sup>192</sup>Ir, secondary charged particle equilibrium can be assumed.<sup>4,27</sup> The bounded next flight estimator technique<sup>19</sup> was used to evaluate the dose rate at various points  $P(r, \theta)$  [Fig. 1(a)] in water surrounding the HDR source. Angular dose profiles  $\Delta \dot{D}(r, \theta)$  for  $\theta$  in the range  $(0^\circ, 180^\circ)$  were evaluated at  $r = 0.25, 1.0, \text{ and } 5$  cm, as well as the radial distribution ( $\theta = \pi/2$ ) for  $r$  in the range  $0.1\text{--}7$  cm. All MCPT results had units cGy/(mCi h) and were used in this form to evaluate DANTSYS accuracy and to calculate the quantities of the model introduced by TG-43.<sup>16</sup> The unit “mCi” refers to the activity contained in the source core, which is proportional to the number of simulated primary photon trajectories. The TG-43 model, starting with a sparsely distributed grid of dose rates derived from measurements or simulations, calculates the dose rate,  $\dot{D}(r, \theta)$ , according to

$$\dot{D}(r, \theta) = S_K \cdot \Lambda \cdot \frac{G(r, \theta)}{G(r_0, \theta_0)} \cdot F(r, \theta) \cdot g(r), \quad r_0 = 1 \text{ cm},$$

$$\theta_0 = 90^\circ, \quad \text{for } ^{192}\text{Ir sources}, \quad (20)$$

where  $S_K$  is the measured air-kerma strength<sup>28</sup> of the source in units of  $U = \text{cGy cm}^2/\text{h}$ , and  $G(r, \theta)$  is a geometry factor. As recommended by the TG-43 report, the unfiltered line source model was used, giving

$$G(r, \theta) = \begin{cases} \frac{\Delta \theta}{L \cdot r \cdot \sin \theta}, & \theta \neq 0, \\ \frac{1}{r^2 - L^2/4}, & \theta = 0, \end{cases} \quad (21)$$

where  $L$  is 0.35 cm, the length of the active source, and  $\Delta \theta$  is the angle (in radians) subtended by the active source with respect to  $P(r, \theta)$ . The dose-rate constant,  $\Lambda$ , for the source and surrounding medium, is evaluated using the MCPT simulation results as follows:

$$\Lambda = \frac{\dot{D}(r_0, \theta_0)}{S_K}. \quad (22)$$

The remaining quantities in Eq. (21) are the anisotropy function,  $F(r, \theta)$ , and the radial dose function,  $g(r)$ . Using the definitions  $F(r, \theta)$  and  $g(r)$  given in the Task Group Report,<sup>16</sup> these dosimetric ratios were evaluated from the calculated  $\dot{D}(r, \theta)$ . More details are given by Williamson and Li.<sup>23</sup>

MCPT simulation was used to evaluate the air-kerma strength per unit contained activity  $S_K$  (in units of  $\text{U mCi}^{-1}$ ) in a 5 m diam air phantom following the same procedure as described in Ref. 23. This quantity is used to normalize the calculated  $\dot{D}(r, \theta)$  allowing clinically relevant absolute absorbed dose rates in water per unit air-kerma strength ( $\text{cGy h}^{-1} \text{U}^{-1}$ ) to be estimated by the simulations.

Our MCPT simulations use point-kerma estimators, which, while providing rigorous benchmarks for assessing the accuracy, do not exploit the cylindrical symmetry of the problem, making efficiency comparisons with DANTSYS meaningless. For evaluating DANTSYS efficiency, we have benchmarked DANTSYS against the EGS4 user code DOSRZ.<sup>29</sup> This is a Monte Carlo code in cylindrical  $R$ - $Z$  geometry, which was used with the same grid cells as in DANTSYS calculations. We did not use EGS4 results for DANTSYS accuracy evaluations for three reasons: (i) the currently available EGS4 version uses Storm and Israel photon cross section data,<sup>30</sup> which may introduce systematic discrepancies due to different cross sections that are difficult to estimate; (ii) the EGS4/DOSRZ results exhibit large statistical uncertainty (exceeding 20%) for grid cells in the 5 cm range along the  $Z$  axis of longitudinal symmetry, which would prevent us from analyzing the DANTSYS accuracy at relevant distances along the  $Z$  axis; and (iii) the MCPT next flight estimators avoid the volume averaging errors associated with approximating kerma at a point with its local voxel average as well as errors associated with the mesh-based geometry modeling of DOSRZ and DANTSYS. DOSRZ uses analog scoring to evaluate the energy deposited in each cylindrical shell detector with no variance reduction techniques applied. Secondary electron transport was suppressed to avoid unnecessary calculations. The number of histories was selected in such a way as to achieve maximum

standard deviation of about 2% in more than 99% of the volume elements of a 20 cm diam by 20 cm height scoring grid.

## 2. DANTSYS multigroup discrete ordinates calculations

The DANTSYS code package<sup>15</sup> used in our studies is a modular computer program designed to solve the time-independent, multigroup discrete ordinates form of the linear transport equation in various geometries for neutral particles. In principle, it could be extended to model electron and coupled photon–electron–positron transport. However, this extension is not straightforward and would require further development.<sup>3</sup> Thus, we apply DANTSYS for modeling photon transport only. For the low-energy photons common in brachytherapy, this still provides a practical dosimetry tool due to the charged particle equilibrium.<sup>4,27</sup> The TWODANT Solver module solves the two-dimensional transport equation using the diamond differencing or adaptive weighted diamond differencing<sup>31</sup> (AWDD) method for space/angle discretization to eliminate negative flux fixups. The diffusion synthetic acceleration<sup>32</sup> (DSA) method is used to accelerate the convergence of the iteration process.

TWODANT was used to solve the two-dimensional cylindrical  $R$ - $Z$  geometry equivalent of Eq. (15) for the  $^{192}\text{Ir}$  HDR source. The finite-difference spatial approximation of the source geometry is shown in Fig. 1(b). A reflection boundary condition<sup>2,15</sup> was assumed along the  $Z$  axis of rotational symmetry, together with a vacuum boundary conditions along the outer surface of the water phantom. Variable voxel sizes along the  $R$  axis, all smaller than 0.3 mean free paths (mfp) for photons with energy 353 keV (the weighted average energy of the  $^{192}\text{Ir}$  spectrum used), were applied. Small voxel sizes are needed to model the source geometry accurately (less than 0.1 mfp in the vicinity and inside the source). The ratio of the  $Z$ -axis to  $R$ -axis voxel dimensions (the aspect ratio) varied from 2:1 near the source to 25:1 at the periphery of the water phantom in the vicinity of the  $R$  or  $Z$  axis. The resulting voxel structure contained 39 voxels along the  $R$  and 136 voxels along the  $Z$  axis. TWODANT's ray-tracing first collision source option<sup>33</sup> was used to mitigate the ray effects. With this method, primary photons (i.e., due to source decay) have their trajectory origin and direction cosines determined by stochastic sampling. The trajectory is then followed throughout the geometry grid, and the flux moments [Eq. (8)] in each grid cell are calculated. The resulting precalculated primary flux distribution is used to generate a broadly distributed first collision source for further discrete ordinate calculations of the scattered flux and related kerma. Between 2 500 000 (with  $S_{16}$ ) and 13 800 000 ( $S_{40}$ ) ray-tracing histories were used to create the first collision source. The statistical uncertainty of the primary flux evaluation was less than 3%, except for the very small mesh cells near the  $Z$  axis of rotational symmetry, where it was between 3 to 30 times larger due to the very small solid angles subtending the spatial grid cells along the  $Z$  axis. The results and discussion in sec. III show the relevance of the ray tracing implementation

in mitigating the ray effects. Quadrature sets containing 36 (denoted as  $S_{16}$ ), 55 ( $S_{20}$ ), 120 ( $S_{30}$ ), and 220 ( $S_{40}$ ) angles per octant were used to evaluate the effect of quadrature on the accuracy and efficiency of the DANTSYS calculations.

We used the high-resolution application-independent 210-energy group photon cross section library<sup>12</sup> (referred to below as G-210). Its very fine energy bin structure eliminates the need for weighting functions to accurately represent group fluxes and cross sections and effectively removes errors associated with the multigroup approximation.<sup>14</sup> G-210 was developed as an application-independent cross section library for the assessment of DOM accuracy and is not intended for use in practical treatment planning. The library contains photon cross sections over the energy range 1 keV–1.5 MeV. Similar to the MCPT cross section data, it was derived from DLC-146, and hence any systematic discrepancies in our calculations due to a different cross section origin are avoided. G-210 contains the scattering cross section matrix coefficients allowing up to fifth degree ( $P_5$ ) Legendre polynomial expansion of the cross section angular dependency [see Eqs. (4)–(5)]. Following the results in Ref. 14, we used  $P_3$  angular polynomial expansion for all calculations.

The multigroup approximation of the  $^{192}\text{Ir}$  spectrum and the appropriate normalization was determined using the procedure described in Ref. 13. The highest-energy  $^{192}\text{Ir}$  photons appear in the second group of G-210 and hence the solution spanned over 209 groups, starting with group 2. The remaining computational parameters used were the same as the ones used in our previous work.<sup>14</sup>

At the conclusion of each calculation, the DANTSYS EDIT module<sup>15</sup> was employed to convert the flux distributions into kerma by using the G-210 group kerma factors. These results were utilized in the form of two-dimensional absorbed dose rate arrays at the points centered at each voxel of the finite-difference geometry approximation. To obtain DOM dose estimates at points not coinciding with DANTSYS grid points, a bilinear interpolation procedure<sup>14</sup> was employed. It uses the TG-43 geometry factor, Eq. (21), to suppress spatial flux variations due to the inverse square law. DANTSYS evaluation of TG-43 quantities was the same as for MCPT, except that the corresponding DANTSYS values were used. All DANTSYS results were normalized to the units of  $\text{cGy mCi}^{-1} \text{h}^{-1}$ , consistent with our MCPT simulations.

The very small voxel sizes needed to resolve the source geometry, together with the large size of the air phantom used for air-kerma strength calculations, lead to a very large number of voxels since the aspect ratios throughout the system must not exceed 30:1 to accurately calculate the scattered contribution to the air kerma of less than 7%. This, and the use of G-210, leads to a highly intensive computational effort for simulations. To avoid this largely unnecessary effort we used the ONEDANT DANTSYS solver module in one-dimensional spherical geometry. It solves the one-dimensional transport equation (15) with the use of a diffusion acceleration scheme.<sup>32</sup> The HDR source was modeled in the center of a 5 m diameter air sphere. The source core and capsule were approximated by spherical shells of

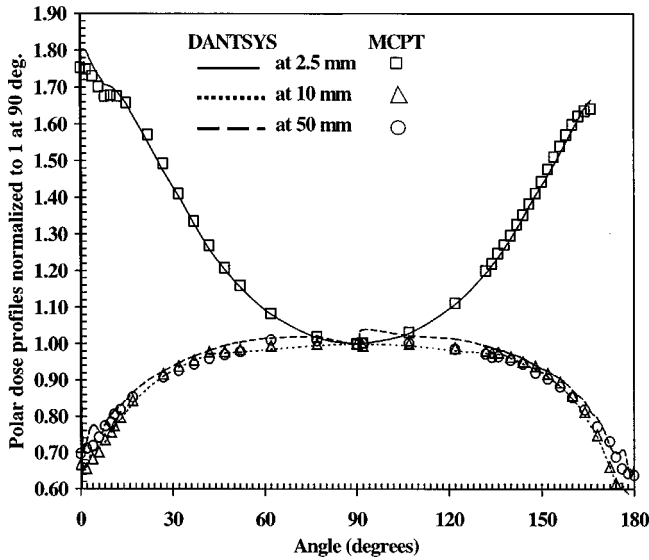


FIG. 2. Polar dose profiles  $\hat{D}(r, \theta)$  normalized to unity at  $\theta = \pi/2$  DANTSYS (curves) and MCPT (symbols) calculations.  $S_{30}$  (120 angles per octant) used for DANTSYS calculations.

the same diameter and material composition as in the underlying MCPT geometric model. The problem geometry was divided into 257 radial elements and the standard DANTSYS  $S_{48}$  angular quadrature (48 angular directions and weights) was used in the simulation.

III. RESULTS AND DISCUSSION

Figure 2 shows the polar dose rate profiles  $\hat{D}(r, \theta)$  for the  $^{192}\text{Ir}$  HDR source as obtained by our MCPT and DANTSYS simulations. Each profile is normalized to unity on the transverse axis ( $\theta = 90^\circ$ ). The apparent maxima at angles  $\theta$  of  $0^\circ$  and close to  $180^\circ$  for the 2.5 mm curve are due to the breakdown of the inverse square law near the ends of the extended

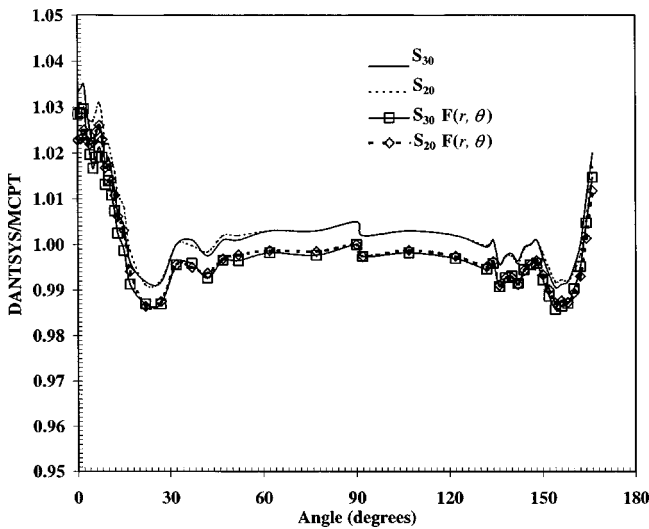


FIG. 3. DANTSYS results relative to MCPT as a function of angle at  $r = 2.5$  mm for absorbed dose distributions  $\hat{D}(r, \theta)$  (curves), and for the angular anisotropy function  $F(r, \theta)$  (curves with symbols).  $S_{30}$  (120 angles per octant) and  $S_{20}$  (55 angles per octant) used for DANTSYS calculations.

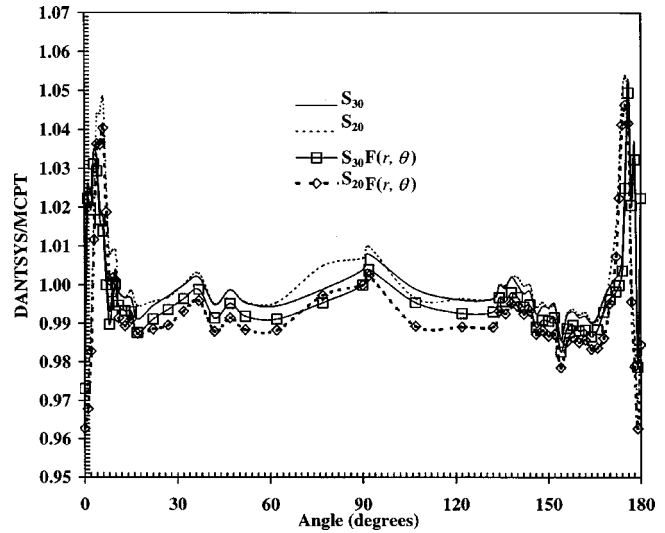


FIG. 4. The same as in Fig. 3 except for the distance  $r = 10$  mm.

radioactivity distribution. The figure shows the excellent agreement between DANTSYS and MCPT for all angles and distances shown.

Similar to our previous work,<sup>14</sup> we used two methods for quantifying the accuracy of DANTSYS. The graphical method is illustrated by Fig. 3, which shows the ratio of the absorbed dose per unit contained activity in water calculated by DANTSYS relative to that calculated by MCPT as a function of angle at a distance 2.5 mm from the source center when  $S_{20}$  and  $S_{30}$  angular quadratures are used in the DANTSYS simulations. The comparison between the angular anisotropy functions  $F(2.5 \text{ mm}, \theta)$  evaluated using DANTSYS and MCPT absorbed dose rate estimates is also shown. Figures 4 and 5 show the same with the only difference being that the evaluation is made at distances 10 and 50 mm, respectively. Similarly, Fig. 6 shows DANTSYS relative to MCPT dose results along the plane transverse to the source as a function of distance from the source center. The figure also includes a compari-

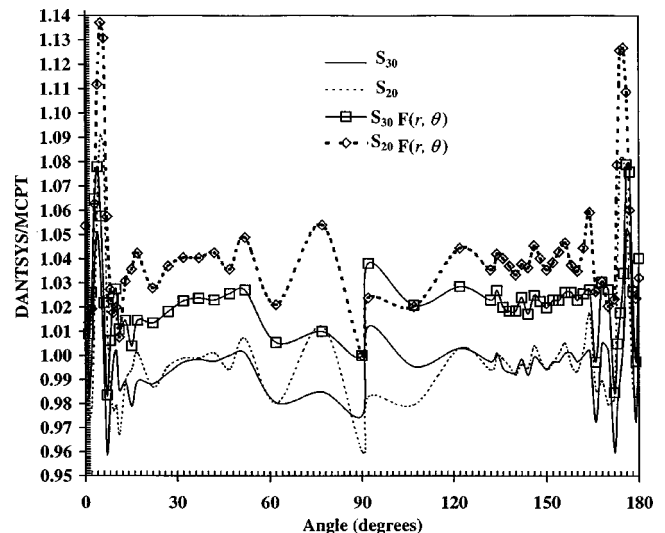


FIG. 5. The same as in Fig. 3 except for the distance  $r = 50$  mm.

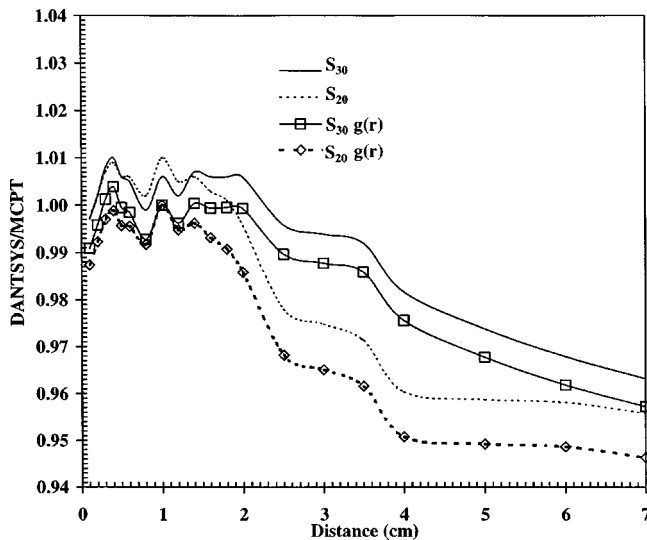


FIG. 6. DANTSYS absorbed dose distribution relative to MCPT within a 70 mm distance from the source center in the plane transverse to the source. DANTSYS simulations with  $S_{30}$  and  $S_{20}$  angular quadratures.  $g(r)$  denotes the DANTSYS/MCPT ratio for the radial dose function.

son between the radial dose function  $g(r)$  evaluated by DANTSYS and MCPT. In addition, DANTSYS accuracy relative to MCPT is quantified by the root mean square error (RMS),

$$RMS(\%) = \sqrt{\frac{1}{N} \sum_{k=1}^N \left[ 1 - \frac{\dot{D}_{W,k}^{DANT}}{\dot{D}_{W,k}^{MCPT}} \right]^2} \cdot 100, \quad (23)$$

where  $\dot{D}_{W,k}^{DANT}$  is the DANTSYS calculated absorbed dose rate per unit contained activity in water at a point  $(r, \theta_k)$  (for polar profile analyses) or  $(r_k, 90^\circ)$  (for radial distributions) and  $\dot{D}_{W,k}^{MCPT}$  is the corresponding MCPT value.  $N$  is the number of MCPT estimator points used in the comparison.

The figures demonstrate the excellent consistency between DANTSYS and MCPT calculations. The presented comparison of the polar profiles in Figs. 3–5 shows the following.

- (i) Except for angles within  $3^\circ$ – $5^\circ$  of the  $Z$  axis of rotational symmetry, the observed discrepancies are less than 4% ( $<2$  standard deviations of MCPT results) for

$S_{30}$ , and 5% (2.5 standard deviations) for  $S_{20}$  at all distances analyzed. Overall, the discrepancies increase slightly when the number of angles in the angular quadrature is reduced. Except in the vicinity of the  $Z$  axis, the difference between the  $S_{30}$  and  $S_{20}$  results is less than 2% due to the effective elimination of the ray effects by the ray tracing first collision source techniques.

- (ii) The discrepancies very close to the  $Z$  axis ( $\theta$  smaller than  $5^\circ$ ) are somewhat larger at all distances studied and increase when lower-order angular quadrature sets are used. A major cause is ray effects that are difficult to mitigate close to the axis of rotational symmetry. In addition, TWODANT’s first collision source algorithm performs poorly in this region, as discussed below. Thus, angular quadratures with a larger number of angles and corresponding weights have to be used together with the ray tracing first collision source technique in order to obtain better accuracy in the vicinity of the  $Z$  axis.
- (iii) The DANTSYS evaluation of the angular anisotropy function, closely follows (within 2%) the corresponding evaluation of the actual dose distributions. The discrepancies occur since the evaluation of the ratio  $\dot{D}(r, \theta)/\dot{D}(r, \pi/2)$  depends on the angular quadrature used.

Similar conclusions apply to the results for transverse-axis distribution comparison, as shown in Fig. 6.

Table I gives the RMS deviations of DANTSYS relative to MCPT results as a function of angular quadrature used in the calculations. For comparison, the table also shows errors with the first collision source disabled (“no ray”). The data in the table show that:

- (i) Very close to the source, the use of  $S_{16}$ – $S_{40}$  are equally accurate. With increasing distance, however, quadrature sets larger than  $S_{16}$  are necessary for acceptable accuracy.
- (ii) The “no ray” column results demonstrate that by simply increasing the order of angular quadrature one

TABLE I. The RMS difference (percentage points) of DANTSYS absorbed dose results relative to MCPT at various distances and angular quadrature sets. The RMS difference for the polar profiles at  $r=2.5$ , 10, and 50 mm distance from the source center, are evaluated at 47 angles (at 2.5 mm) and 57 angles (at 10 and 50 mm). The RMS values for the transverse axis distribution between 1 and 70 mm are calculated over 20 points along the transverse axis. The MCPT standard deviation was in the range of 0.5%–1.0% at 2.5 mm, 1.0%–2% at 10 mm, and 1.5%–2.5% at 50 mm. The standard deviation of the MCPT results along the transverse axis was varying between 0.43% (at 1 mm) and 2.75% (at 70.0 mm).

Angular quadrature	RMS (%)							
	36 angles and weights ( $S_{16}$ )		55 angles and weights ( $S_{20}$ )		120 angles and weights ( $S_{30}$ )		210 angles and weights ( $S_{40}$ )	
	Ray tracing	No ray	Ray tracing	No ray	Ray tracing	No ray	Ray tracing	No ray
At 2.5 mm	1.76	9.93	1.44	9.39	1.42	8.95	1.31	9.02
At 10 mm	3.16	38.7	1.88	28.0	1.48	19.8	2.12	14.0
At 50 mm	16.4	40.0	2.70	29.4	2.63	19.9	1.39	15.3
Transverse axis	2.88	32.5	2.16	37.7	1.40	18.4	0.98	12.5

TABLE II. Dose-rate constant  $\Lambda$  calculated by DANTSYS with various angular quadratures using the ONEDANT value of  $S_K = 3.69 \text{ U mCi}^{-1}$  for the HDR source air-kerma strength per unit contained activity, and a comparison with the MCPT calculated value.

	DANTSYS								
	MCPT	$S_{16}$		$S_{20}$		$S_{30}$		$S_{40}$	
		Ray	No ray						
$\Lambda$ ( $\text{cGy cm}^2 \text{h}^{-1} \text{U}^{-1}$ )	1.111	1.094	1.220	1.101	1.227	1.098	1.187	1.097	1.160
% difference		-1.5%	+9.8%	-0.91%	+10.4%	-1.2%	+6.9%	-1.3%	+4.4%

can reduce the error and improve the DOM accuracy without using a first collision source technique, as the theory indicates (see Sec. II A.) The error reduction, however, increases slowly with increasing the order of angular quadrature, indicating that this strategy for minimizing ray effects is not practical. The implementation of the first collision source mitigation technique reduces RMS error by a factor of 10 or more in all cases, allowing the use of coarser quadrature sets without compromising the accuracy.

The ONEDANT air-kerma strength per unit contained activity of  $S_K = 3.69 \mu\text{Gy m}^2 \text{h}^{-1} \text{mCi}^{-1}$  closely approximates the MCPT value of  $3.63 \mu\text{Gy m}^2 \text{h}^{-1} \text{mCi}^{-1}$ . This result was achieved in 35 s of CPU time on our SGI RS 10000 workstation and demonstrates the ability of one-dimensional DOM calculations to produce accurate estimates in an extremely efficient manner. Table II shows the  $\Lambda$  values calculated by both MCPT and DANTSYS for all angular quadratures, with and without first collision source calculations, and using the ONEDANT  $S_K$  value for DANTSYS estimates. The resultant  $\Lambda$  estimates are in close agreement with those of Williamson and Li<sup>23</sup> and Kirov *et al.*<sup>34</sup> The differences in DANTSYS  $\Lambda$ 's are within 0.6% for all angular quadratures. At the same time, the overall discrepancy of about -1% between DANTSYS and MCPT values is mostly due to the ONEDANT overestimation of  $S_K$  by 1.7%. When no ray effects mitigation technique is used, the result becomes very sensitive to the order of angular quadrature. Even with the highest-order  $S_{40}$  used in this study, the observed discrepancy is a factor of 4 larger relative to the cases when a first collision source calculation is employed.

Table III compares the CPU run times of DANTSYS and EGS4 simulations when based upon geometries that are equivalent in terms of the number and size of 2-D cells. The total CPU times ("ray" row) includes both the CPU time for the first collision source calculation and for the actual DOM iterations ("iteration" column). The number of DOM iterations needed to obtain convergence in each case is given in the "#iter" column. For comparison, the DANTSYS results without a first collision source are also included ("no ray" row). The following is seen.

- (i) When the first collision source is implemented (the "ray" row), two-fold efficiency gains are achievable when  $S_{20}$  or lower-order angular quadratures are used,

while  $S_{30}$  or higher-order angular quadratures lead to equivalent or longer CPU times relative to EGS4/DOSRZ. The iteration CPU time (or total, in the "no ray" row) for various angular quadratures scales with the number of problem phase space cells proportional to the number of angles in the quadrature. Thus, if the size of the problem phase space can be reduced, the iteration time can be reduced proportionally.

- (ii) The number of DOM iterations does not depend on the angular quadrature used with the same geometry representation.
- (iii) The ray-tracing first collision source calculation CPU time takes between 35% ( $S_{16}$ ) and 41% ( $S_{40}$ ) of the total time. The implementation of the first collision source leads to less than 5% reduction in the number of DOM iterations. However, the CPU per iteration is reduced by almost 60%. As a result, the total run time in any of the ray/no ray cases is essentially the same. At the same time, the accuracy analysis (Table I) clearly shows that while increasing the angular quadrature order indeed reduces the MCPT/DANTSYS discrepancies without a first collision source, even the use of  $S_{40}$  gives unsatisfactory results. This, together with the excellent agreement of MCPT and DANTSYS with  $S_{20}$  and using the first collision source option, clearly demonstrate the cost effectiveness of the first collision source implementation relative to simply increasing the order of angular quadrature alone.

Our results demonstrate that the first collision source technique used here effectively reduces the ray effects and allows the use of lower-order angular quadratures without significantly affecting the accuracy. The ray-tracing algorithm currently employed in DANTSYS, however, poorly estimates the first collision source in limited areas along the  $Z$  axis of rotational symmetry. The reason is that the small size of the source modeled leads to a small number of primary photon trajectories intersecting the spatial voxels along the  $Z$  axis, causing poor statistics in the first collision source evaluation. In addition, Table III shows that the ray-tracing calculations may take a significant fraction of the overall DANTSYS run times. These deficiencies of the internal DANTSYS ray-tracing algorithm clearly need to be addressed. The simpler source geometry of a typical brachytherapy problem (at least relative to the reactor physics problems for which DANTSYS was

TABLE III. DANTSYS overall ("total") and iteration CPU times ("iteration") in minutes for different orders of angular quadratures. Results with ("ray") and without ("no ray") a first collision option. A comparison with EGS4/DOSRZ Monte Carlo code. The DOSRZ code was running until the maximal standard deviation (SD%) in 99% of the phantom volume reached the value shown. All times are valid on the SGI RS10000 workstation.

	DANTSYS												EGS4/DOSRZ					
	$S_{40}$ (210 angles per octant)			$S_{30}$ (120 angles per octant)			$S_{20}$ (55 angles per octant)			$S_{16}$ (36 angles per octant)			EGS4/ DANTSYS	Total CPU	Number of histories (millions)	SD %	CPU time (min)	
	DANTSYS CPU (min)	#Iter	Total CPU	DANTSYS CPU (min)	#Iter	Total CPU	DANTSYS CPU (min)	#Iter	Total CPU	DANTSYS CPU (min)	#Iter	Total CPU						
ray	454	267	847	0.62	847	845	1.06	133	85	845	2.12	83	54	846	3.4	70	2.07	282
no ray	450	450	884	0.62	885	885	1.06	125	125	886	2.12	87	87	886	3.4	70	2.07	282

originally designed) makes alternative numerical or analytical approaches (e.g., similar to the parametric<sup>35</sup> or "nearest pixel" nonparametric<sup>36</sup> ray-tracing algorithms) feasible for calculating the first collision source without the difficulties experienced with the standard DANTSYS ray-tracing algorithm.

Overall, the data in Table III indicate that DANTSYS calculations with G-210 do not produce sustainable gains in efficiency and the computational efforts of DOM and Monte Carlo are essentially the same. The major cause of this result is the large number of phase space cells used in DOM calculations, in particular, due to the large number of groups in G-210. The G-210 photon cross section library was designed for DOM accuracy analyses and is clearly not suitable for clinical treatment planning. More recent work demonstrates<sup>37</sup> that for I-125 brachytherapy, a three-group approximation yields acceptable accuracy while yielding efficiency gains of 80 or more. A further reduction in the number of phase space cells may be achieved by the use of higher-order spatial-differencing schemes,<sup>2</sup> which would allow larger voxel sizes and aspect ratios to be used for an accurate solution. The Adaptive Mesh Refinement technique, which allows local grid refinement to minimize the spatial error in regions with steep flux gradients and larger cells in low gradient regions, would relax the spatial grid alignment constraints and avoid the spread of smaller voxel sizes near the source throughout the system. Both approaches potentially lead to a smaller number of spatial voxels and would allow lower-order angular quadratures to be used consistently in the simulations, which, in turn, could further improve DOM efficiency.<sup>18</sup>

#### IV. CONCLUSIONS

In this study we show that the discrete ordinates method, in general, and the DANTSYS code system, in particular, can accurately model photon kerma rate distributions in the vicinity of the <sup>192</sup>Ir HDR source in two-dimensional cylindrical *R-Z* geometry. The DANTSYS results closely approximate the MCPT values with discrepancies smaller than 3%–5% (within two standard deviations of the Monte Carlo results) throughout the modeled phantom, except for limited regions along the *Z* axis of rotational symmetry, where ray effects are observed that are difficult to mitigate with the DANTSYS internal first collision source algorithm. The same accuracy was obtained for the DOM evaluation of the TG-43 anisotropy function,  $F(r, \theta)$ , radial dose function,  $g(r)$ , and the dose-rate constant,  $\Lambda$ , associated with the microSelectron <sup>192</sup>Ir HDR source. The present finite-difference model, together with  $S_{20}$  angular quadrature consisting of 55 directions and associated weights per octant, and the  $P_3$  angular polynomial expansion of the photon scattering anisotropy, was sufficient to achieve the observed accuracy. The DANTSYS ONEDANT one-dimensional DOM solver module provided an accurate estimate of the source air-kerma strength in an extremely efficient manner.

To achieve the above accuracy, the first collision source technique was used to mitigate the strong ray effects. The

DANTSYS Monte Carlo implementation of this algorithm, while effective in mitigating ray effects, does not efficiently estimate primary photon collision density along the source longitudinal axis.

Our high-resolution G-210 multigroup library provides accuracy equivalent to that of a continuous energy MCPT code. However, the large number of groups significantly increases the CPU time and computer memory and is not dramatically more efficient than EGS4 two-dimensional calculations. The comparison with the EGS4 Monte Carlo code using the same geometry representation indicates that some marginal gain in efficiency, of about a factor of 2, is nevertheless achievable. The present results, while not optimized for computational efficiency, demonstrate the accuracy and establish the range of DANTSYS computational parameters needed for successful simulations. They also indicate the large DOM potential for efficiency improvements by reducing the number of discrete phase space cells needed to adequately resolve the source geometry and dose distribution. Future efforts directed toward reducing the number of phase space cells used in the calculations together with optimizing the other necessary features (e.g., the implementation of ray effects mitigation techniques) are expected to allow successful and efficient discrete ordinates applications in brachytherapy.

## ACKNOWLEDGMENT

The present study was supported by the National Institute of Health Grant No. R01 CA46640.

<sup>a</sup>Corresponding author. Phone: (613)-993-2715; fax: (613)-952-9865; electronic mail: daskalov@irs.phy.nrc.ca

<sup>1</sup>E. E. Lewis and W. F. Miller, Jr., *Computational Methods of Neutron Transport* (Wiley, New York, 1984).

<sup>2</sup>R. D. O'Dell and R. E. Alcouffe, "Transport calculations for nuclear reactors," in *CRC Handbook of Nuclear Reactors Calculations*, edited by Y. Ronen (CRC, Boca Raton, 1986), pp. 341–462.

<sup>3</sup>C. R. Drumm, "Multidimensional electron-photon transport with standard discrete ordinates codes," *Nucl. Sci. Eng.* **127**, 1–21 (1997).

<sup>4</sup>R. K. Valicenty, A. S. Kirov, A. S. Meigooni, V. Mishra, R. K. Das, and J. F. Williamson, "Experimental validation of Monte Carlo dose calculations about a high-intensity Ir-192 source for pulsed dose-rate brachytherapy," *Med. Phys.* **22**, 821–829 (1995).

<sup>5</sup>D. W. Nigg, P. D. Randolph, and F. J. Wheeler, "Demonstration of three-dimensional deterministic radiation transport theory dose distributions analysis for boron neutron capture therapy," *Med. Phys.* **18**, 43–53 (1991).

<sup>6</sup>G. J. Storr, "Assessment of ideal neutron beams for neutron capture therapy," *Radiat. Res.* **131**, 235–242 (1992).

<sup>7</sup>J. M. Moran, D. W. Nigg, F. J. Wheeler, and W. F. Bauer, "Macroscopic geometric heterogeneity effects in radiation dose distribution analysis for boron neutron capture therapy," *Med. Phys.* **19**, 723–732 (1992).

<sup>8</sup>D. W. Nigg, "Methods for radiation dose distribution analysis and treatment planning in boron neutron capture therapy," *Int. J. Radiat. Oncol., Biol., Phys.* **28**, 1121–1134 (1994).

<sup>9</sup>J. P. Windham, A. Shapiro, and J. G. Kereiakes, "Calculated neutron dose rates for implantable californium-252 sources," *Phys. Med. Biol.* **17**, 493–502 (1972).

<sup>10</sup>A. Shapiro, B. Schwartz, J. P. Windham, and J. G. Kereiakes, "Calculated neutron dose rates and flux densities from implantable californium-252 point and line sources," *Med. Phys.* **3**, 241–247 (1976).

<sup>11</sup>N. E. Hertel and W. E. Murphie, "The use of neutron and gamma ray

spectral measurements and calculations to obtain dosimetric information for DT neutrons," *Med. Phys.* **10**, 66–74 (1983).

<sup>12</sup>Y. Uwamino, T. Nakamura, and T. Ohkubo, "Measurement and calculation of neutron leakage from a medical electron accelerator," *Med. Phys.* **13**, 374–384 (1986).

<sup>13</sup>G. M. Daskalov, R. S. Baker, R. C. Little, D. W. O. Rogers, and J. F. Williamson, "Multigroup discrete ordinates photon transport calculations of water kerma for brachytherapy applications," in the *Proceedings of the ANS Topical Conference*, 19–23 April 1998, Nashville, TN, 1998, Vol. 2, pp. 261–268.

<sup>14</sup>G. M. Daskalov, R. S. Baker, R. C. Little, D. W. O. Rogers, and J. F. Williamson, "Two-dimensional discrete ordinates photon transport calculations for brachytherapy dosimetry applications," *Nucl. Sci. Eng.* **134**, 121–134 (2000).

<sup>15</sup>R. E. Alcouffe, R. S. Baker, F. W. Brinkley, D. R. Marr, R. D. O'Dell, and W. F. Walters, "DANTSYS: A diffusion accelerated neutral particle transport code system," LA-12969-M, Los Alamos National Laboratory, Los Alamos, NM, June 1995.

<sup>16</sup>R. Nath, L. L. Anderson, G. Luxton, K. A. Weaver, J. F. Williamson, and A. S. Meigooni, "Dosimetry of interstitial brachytherapy sources: Recommendations of the AAPM Radiation Committee Task Group No. 43," *Med. Phys.* **22**, 209–234 (1995).

<sup>17</sup>D. E. Cullen, "Nuclear cross section preparation," in *CRC Handbook of Nuclear Reactors Calculations*, edited by Y. Ronen (CRC, Boca Raton, 1986), pp. 13–131.

<sup>18</sup>R. E. Alcouffe, E. W. Larsen, W. F. Miller, and B. R. Wienke, "Computational efficiency of numerical methods for multigroup, discrete-ordinates neutron transport equations: The slab geometry case," *Nucl. Sci. Eng.* **71**, 111–127 (1979).

<sup>19</sup>J. F. Williamson, "Monte Carlo evaluation of kerma at a point for photon transport problems," *Med. Phys.* **14**, 567–576 (1987).

<sup>20</sup>Z. Li and J. F. Williamson, "Volume-based geometric modeling for radiation transport calculations," *Med. Phys.* **19**, 667–678 (1992).

<sup>21</sup>J. F. Williamson and A. S. Meigooni, "Quantitative dosimetry methods for brachytherapy," in *Brachytherapy Physics*, edited by J. F. Williamson, B. T. Thomadsen, and R. Nath (Medical Physics Publishing Co, Madison, 1995).

<sup>22</sup>J. F. Williamson, H. Perera, Z. Li, and W. R. Lutz, "Comparison of Calculated and measured heterogeneity correction factors for <sup>125</sup>I, <sup>137</sup>Cs, and <sup>192</sup>Ir brachytherapy sources near localized heterogeneities," *Med. Phys.* **20**, 209–222 (1993).

<sup>23</sup>J. F. Williamson and Z. Li, "Monte Carlo aided dosimetry of the microselectron pulsed and high dose-rate <sup>192</sup>Ir Sources," *Med. Phys.* **22**, 809–819 (1995).

<sup>24</sup>G. P. Glasgow and T. L. Dilman, "Specific  $\gamma$ -ray constant and exposure constant of <sup>192</sup>Ir," *Med. Phys.* **6**, 49–52 (1979).

<sup>25</sup>RSIC Data Library DLC-146, "HUGO-VI: Photon interaction data in ENDF/B-VI Format," RSICC, ORNL, Oak Ridge, TN, August 1989.

<sup>26</sup>J. H. Hubbell and S. M. Seltzer, "Tables of x-ray mass attenuation coefficients and mass energy-absorption coefficients 1 keV to 20 MeV for elements Z=1 to 92 and 48 Additional substances of dosimetric interest," NISTIR 5632, May 1995.

<sup>27</sup>F. H. Attix, *Introduction to Radiological Physics and Radiation Dosimetry* (Wiley, New York, 1986), Chap. 4.

<sup>28</sup>R. Nath, L. Anderson, D. Jones, C. Ling, R. Loevinger, J. F. Williamson, and W. Hanson, *Specification of Brachytherapy Source Strength: A Report by Task Group 32 of the American Association of Physicists in Medicine*, AAPM Report 21 (American Institute of Physics, Woodbury, 1987).

<sup>29</sup>W. R. Nelson, A. Hirayama, and D. W. O. Rogers, "The EGS4 code system," Stanford Linear Accelerator Center Report SLAC-265, Stanford, CA, 94305, 1985.

<sup>30</sup>E. Storm and H. I. Israel, *Nucl. Data, Sect. A* **7**, 565–681 (1970).

<sup>31</sup>R. E. Alcouffe, "An adaptive weighted diamond differencing method for three-dimensional XYZ geometry," *Trans. Am. Nucl. Soc.* **68A**, 206–209 (1993).

<sup>32</sup>R. E. Alcouffe, "Diffusion synthetic acceleration methods for the diamond-differencing discrete-ordinates equations," *Nucl. Sci. Eng.* **64**, 344–355 (1977).

<sup>33</sup>R. S. Baker, "A stochastic first collision source for TWODANT," *8th International Conference On Radiation Shielding*, Arlington, TX, 1994, Vol. 1, pp. 157–164.

- <sup>34</sup>A. S. Kirov, J. F. Williamson, A. S. Meigooni, and Y. Zhu, "TLD, diode and Monte Carlo dosimetry of an  $^{192}\text{Ir}$  Source for high dose-rate brachytherapy," *Phys. Med. Biol.* **40**, 2015–2036 (1995).
- <sup>35</sup>R. L. Siddon, "Fast calculation of the exact radiological path for a three-dimensional CT array," *Med. Phys.* **12**, 252–255 (1985).
- <sup>36</sup>M. W. Frandsen, D. E. Wessol, F. J. Wheeler, R. S. Babcock, G. H. Harkin, and J. D. Starkey, "Rapid interrogation for a uniform volume element-based Monte Carlo particle transport simulations," in the *Proceedings of the ANS Topical Conference*, 19–23 April 1998, Nashville, TN, 1998, Vol. 2, pp. 84–94.
- <sup>37</sup>G. M. Daskalov, R. S. Baker, D. W. O. Rogers, and J. F. Williamson, "Multigroup discrete ordinates modeling of  $^{125}\text{I}$  6702 seed dose distribution using a broad energy-group cross section representation," submitted to *Phys. Med. Biol.*; The abstract of the presentation on the same topic at AAPM Annual Meeting in Nashville, TN, July 25–29, 1999, *Med. Phys.* **26**, 1141 (1999).